Coulomb-potential effects in nonsequential double ionization under elliptical polarization

MingYan Wu,[1,2] YanLan Wang,[1,2] and XiaoJun Liu[1,*]

[1]*State Key Laboratory of Magnetic Resonance and Atomic and Molecular Physics, Wuhan Institute of Physics and Mathematics, Chinese Academy of Sciences, Wuhan 430071, China*

[2]*Graduate School of Chinese Academy of Sciences, Beijing 100080, China*

WeiDong Li

Institute of Theoretical Physics and Department of Physics, Shanxi University, 030006 Taiyuan, China

XiaoLei Hao and Jing Chen[†]

HEDPS, Center for Applied Physics and Technology, Peking University, 100084 Beijing, China, and Institute of Applied Physics and Computational Mathematics, P.O. Box 100088 Beijing, China

(Received 17 July 2012; revised manuscript received 30 December 2012; published 25 January 2013)

Using a semiclassical model, we evaluate the correlated electron momentum distribution from nonsequential double ionization (NSDI) of neon in an elliptically polarized laser field. The momentum distribution pattern exhibits a nontrivial change with the increase of the laser ellipticity, which can be understood as a combined effect of the extra laser electric field and the ionic Coulomb potential on the tunnel-ionized electron trajectory. Especially for large ellipticities ($\epsilon > 0.2$), multiple return collision trajectory contributes dominantly to the NSDI yield and determines the correlated electron momentum distribution, revealing an indispensable role of ionic Coulomb potential in NSDI dynamics under elliptical polarization. Moreover, the nontrivial evolution of the correlated electron momentum distribution with the ellipticity revealed in our model should be testable by a realistic experiment.

DOI: 10.1103/PhysRevA.87.013431 PACS number(s): 33.80.Rv, 34.80.Gs, 42.50.Hz

I. INTRODUCTION

The study on interaction of atoms and molecules with intense laser fields has been a forefront topic in atomic and molecular physics for the last three decades. A large variety of interesting strong-field atomic phenomena, namely multiphoton ionization (MPI), above-threshold ionization (ATI), high-order harmonic generation (HHG), and multiple ionization and others, have emerged [1]. Among all those, the nonsequential double ionization (NSDI) draws unusual attention because an anomalously high degree of electron correlation was involved in this process, thus providing an ideal prototype to investigate the electron correlation effect in laser-driven atomic phenomena (For recent reviews, see, e.g., [2–4].)

It is nowadays widely accepted that the underlying mechanism for atomic NSDI in a strong laser field is based on the electron recollision process (also called as three-step process) [5]. In this process, the outmost electron in an atom becomes free by tunneling through the distorted Coulomb-potential barrier, created by the external laser electric field, is accelerated in the laser field, gains energy, and can be driven back to the parent ion when the field reverses its direction. Upon recollision the second electron (still bound up to this point) may gain enough energy via electron correlation interaction and both electrons become ionized.

According to this simple electron recollision scenario, there are little or no NSDI events when the laser field is elliptically polarized or circularly polarized since the first tunnel-ionized electron cannot return to its parent ion due to the presence of the additional transverse electric field component. Indeed, this was confirmed by earlier experiments [6]. However, later experiments exhibited facts that are in contradiction with this expectation. For example, characteristic NSDI events have been observed in the molecules O_2 [7] and NO [8] and atomic Mg [9] under circular polarization. These unexpected observations have attracted increasing attention of theorists to the underlying physical mechanism behind NSDI under elliptical and circular polarization.

On the basis of a completely classical model, Wang and Eberly [10,11] have shown that NSDI does exist with elliptical and circular polarization and the successful NSDI events come from electron recollision through elliptical trajectories. Hao *et al.* [12] investigated NSDI of noble gas neon in an elliptically polarized laser field with the help of the semiclassical model, which, opposed to the completely classical model, considers the quantum tunneling as the initiator of NSDI. Their calculation reproduced the earlier experimental data [6] and predicted the frequency dependence of the ratio of the doubly charged ion with respect to the singly charged ion. Very recently, the semiclassical model has also been employed by Fu *et al.* [13] to study the abnormal NSDI behavior of atomic magnesium under circular polarization and, by adopting a screened Coulomb potential, the experimental data has been well reproduced.

So far, most studies on NSDI under elliptical or circular polarization were focused on the ion yield production in the NSDI process. With the advent of a sophisticated cold target recoil ion momentum spectroscopy (COLTRIMS) technique [14], it is now possible to measure the differential recoil ion momentum and correlated electron momentum distribution, which could provide much more detailed insight into the NSDI process. Surprisingly, though there are abundant differential data available with a linearly polarized laser field, the COLTRIMS measurement under elliptical and circular polarized light is still lacking [15]. Theoretically, the differential ion momentum and correlated electron momentum

*xjliu@wipm.ac.cn
†chen_jing@iapcm.ac.cn

distribution in NSDI under elliptical polarization has been for the first time calculated by Shvetsov-Shilovski *et al.* [16] with a semiclassical model. Their results showed significant variations of symmetry patterns in the ion and electron momentum distributions with the increase of the ellipticity. The authors also found that, due to the presence of the transverse electric field component, longer orbits start to dominate the double ionization yield when the ellipticity is larger than 0.3. Note that in their model, the strong-field approximation (SFA), in which the effect of atomic Coulomb potential on the electrons is completely ignored, has been employed. Considering the accumulated evidence of the decisive role of the ionic Coulomb field in ionized electron dynamics [17,18], NSDI dynamics under elliptical polarization may also be influenced by the ionic Coulomb potential, and a comprehensive understanding of NSDI thus requires a proper treatment of the Coulomb interaction in the model calculation.

In this paper, we employ a three-dimensional semiclassical model, in which the effect of ionic Coulomb potential on the ionized electron dynamics is fully considered, to investigate the correlated electron momentum distribution in NSDI under an elliptically polarized laser field. We find that, with the ellipticity of the laser field increased from 0.0 to 0.3, the correlated electron momentum distribution from NSDI varies significantly. Moreover, our analysis reveals that the ionic Coulomb potential, in addition to the transverse laser field, plays a significant role in determining the correlated electron momentum distribution pattern. The evolution of the correlated electron momentum spectra with the laser ellipticity can be understood by a combined effect of the Coulomb field and the additional electric field on the tunnel-ionized electron dynamics.

II. THEORETICAL MODEL

In this work, the semiclassical model [19,20] is used to describe the NSDI process of neon. In this model, the most loosely bounded electron is assumed to release into the continuum by tunneling through the potential barrier created by the superposition of the atomic Coulomb potential and the laser electric field. Thereafter, the motion of this tunnel-ionized electron and another bounded electron are completely determined by the classical Newtonian equation of motion (atomic units are used throughout the paper unless stated otherwise),

$$\frac{d^2\mathbf{r}_i}{dt^2} = \mathbf{E}(t) - \nabla\left(V_{ne}^i + V_{ee}\right), \tag{1}$$

where $\mathbf{E}(t) = (E_x(t), 0, E_z(t))$ is the elliptically polarized electric field. $E_x(t) = a(t)E_{0x}\sin\omega t$ and $E_z(t) = a(t)E_{0z}\cos\omega t$ with the pulse envelope

$$a(t) = \begin{cases} 1, & t \leqslant 10T, \\ \cos^2\frac{(t-10T)\pi}{6T}, & 10T < t \leqslant 13T, \\ 0, & t > 13T, \end{cases} \tag{2}$$

where T is the optical period and ω is the laser frequency. The ellipticity of the laser field is defined as $\varepsilon \equiv E_{0x}/E_{0z}$. The tunnel-ionized electron and the bounded electron, with ionization potentials of I_{p1} and I_{p2}, are denoted by $i = 1$ and 2, respectively. The nuclear binding potentials for the two electrons, V_{ne}^i, and the interaction potential between the electrons, V_{ee}, are given by

$$V_{ne}^i = -\frac{2}{|\mathbf{r}_i|} \quad \text{and} \quad V_{ee} = \frac{1}{|\mathbf{r}_1 - \mathbf{r}_2|}, \tag{3}$$

where $\mathbf{r}_i$ denotes the distance between the ith electron and the parent ionic core.

In order to solve Eq. (1), the initial conditions for the two electrons, i.e., the initial positions and velocities, has to be setup. The initial position of the first electron can be obtained from the tunnel ionization theory. The Schrödinger equation for an electron in a uniform field E can be reformulated as [21,22]

$$\frac{d^2\phi}{d\eta^2} + \left(\frac{I_{p1}}{2} + \frac{1}{2\eta} + \frac{1}{4\eta^2} + \frac{E\eta}{4}\right)\phi = 0 \tag{4}$$

in parabolic coordinates. Physically, Eq. (4) describes the electron tunneling through a one-dimensional potential $U(\eta) = -1/4\eta - 1/8\eta^2 - E\eta/8$ with energy $K = I_{p1}/4$. Thus, the outer turning point η_0 of the potential $U(\eta)$, viz., the "tunnel exit," can be determined by $U(\eta) = K$ [21]. In our calculation for an elliptically polarized field, the initial condition of the first electron is determined as follows: The electric field of the laser is confined in the x-z plane. At each tunneling moment t_0, the z axis is rotated to be parallel to the instantaneous electric field. The initial condition is obtained in the rotated coordinates the same as in the linearly polarized field and then projected to the original coordinates. For the initial position of the first electron, the obtained coordinates in the rotated coordinates are $x'_{10} = y'_{10} = 0$ and $z'_{10} = -\frac{1}{2}\eta_0$ and hence the coordinates in the original coordinates are $x_{10} = -\frac{1}{2}\eta_0\sin\{\arctan[\varepsilon\tan(\omega t_0)]\}$, $y_{10} = 0.0$, and $z_{10} = -\frac{1}{2}\eta_0\cos\{\arctan[\varepsilon\tan(\omega t_0)]\}$, where t_0 represents the ionization time. For the initial velocity of the first electron in the rotated coordinates, the initial longitudinal velocity at the ionization time t_0 is assumed to be zero. While a nonzero initial velocity $v_{\rm per}$ perpendicular to the laser polarization direction is introduced in the calculation, the corresponding initial velocities are $v'_{1x0} = v_{\rm per}\cos\theta$, $v'_{1y0} = v_{\rm per}\sin\theta$, and $v'_{1z0} = 0$, where θ is the angle between $v_{\rm per}$ and x' axis in the rotated coordinates. Projection into original coordinates gives the initial velocity of the first electron: $v_{1x0} = v_{\rm per}\cos\theta\cos\{\arctan[\varepsilon\tan(\omega t_0)]\}$, $v_{1y0} = v_{\rm per}\sin\theta$, and $v_{1z0} = -v_{\rm per}\cos\theta\sin\{\arctan[\varepsilon\tan(\omega t_0)]\}$. The weight of each trajectory is evaluated by $w(t_0, v_{\rm per}) = w(0)\overline{w(1)}$ [21], where

$$w(0) = \frac{4(2|I_{p1}|)^2}{E}\exp[-2(2|I_{p1}|)^{\frac{3}{2}}/3E] \tag{5}$$

and

$$\overline{w(1)} = \frac{v_{\rm per}(2|I_{p1}|)^{\frac{1}{2}}}{E\pi}\exp\left[-v_{\rm per}^2(2|I_{p1}|)^{\frac{1}{2}}/E\right]. \tag{6}$$

For the second electron (bounded electron), the initial conditions are determined by assuming that the electron is in the ground state of the singly charged ion and its initial distribution is a microcanonical distribution [23].

In the model calculation, more than 5×10^6 initial points are randomly distributed in the parameter space $-\pi/2 < \omega t_0 < \pi/2$, $v_{\rm per} > 0$, and $0 < \theta < 2\pi$ for the first electron

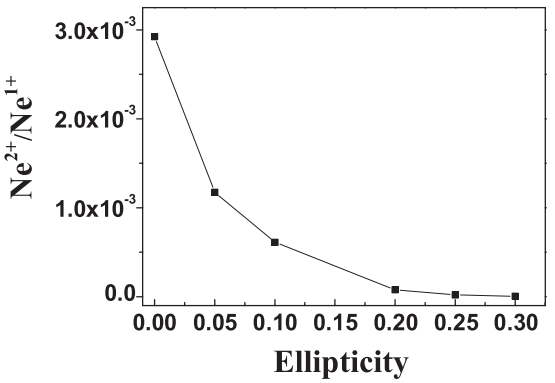

FIG. 1. Ellipticity dependence of the ratio Ne^{2+}/Ne^{1+}. The laser intensity $I = 5 \times 10^{14}$ W/cm^2 and the laser wavelength $\lambda = 800$ nm.

and in the microcanonical distribution for the second electron. The evolution of this two-electron system is traced until the end of the laser field according to the classical Newton equation (1) and double-ionization events are identified by an energy criterion.

III. NUMERICAL RESULTS AND DISCUSSION

In Fig. 1, we plot the calculated ratio of Ne^{2+}/Ne^{1+} as a function of ellipticity. The laser intensity is chosen as $I = 5 \times 10^{14}$ W/cm^2 and the laser wavelength $\lambda = 800$ nm. It is found that with increasing ellipticity, the ratio of Ne^{2+}/Ne^{1+} decreases rapidly and this feature is in good agreement with Ref. [12]. Compared with the case of $\varepsilon = 0$, the returned electron is driven away by extra electric field in the transverse direction. As a consequence, the recollision probability decreases with increasing ellipticity, leading to the drop of the ratio Ne^{2+}/Ne^{1+}.

Moreover, we depict in Fig. 2 the calculated correlated electron momentum distributions from NSDI of the noble gas neon, in the direction parallel to the major axis (i.e., z axis in our case) of elliptically polarized laser field with ellipticities between $\varepsilon = 0$ and $\varepsilon = 0.30$. In general, the electron momentum distribution under elliptical polarization exhibits a similar pattern to that with linear polarization although the total amount of NSDI events drop rapidly with the ellipticity. A most prominent feature is that the electron pairs are mainly located in the first and third quadrants, suggesting that the electron impact ionization (EII) dominates in NSDI [24–26] at the laser parameters employed in this work. However, a closer inspection reveals some significant differences in the electron momentum distributions from Figs. 2(a) to 2(f), with the increasing ellipticity. In the case of the linear polarization [Fig. 2(a)], the proportions of electron pairs in the first and third quadrants are similar but rather favor the third quadrant. Note that the ratio between the weights in the first and the third quadrants is about 2:3. While for small ellipticities, e.g., $\varepsilon = 0.05$ and 0.10 [see Figs. 2(b) and 2(c)], more electron pairs appear in the third quadrant than in the first quadrant. In contrast, for large ellipticities in Figs. 2(d)–2(f), the electron pairs tend to be accumulated in the first quadrant. This becomes most significant as the ellipticity increases to 0.30, for which the electron pairs in the first quadrant are much more than that in the third quadrant.

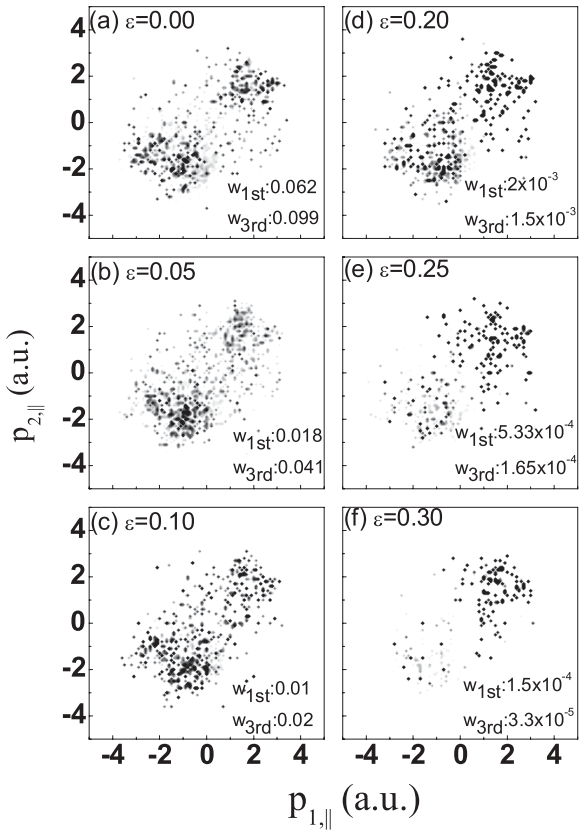

FIG. 2. Correlated electron momentum distributions from NSDI of nobel gas neon in the direction of major axis of elliptically polarized laser field with ellipticities from 0 to 0.30. W_{1st} and W_{3rd} represent the total weights of electron pairs in the first and third quadrants, respectively.

To understand the origin of the change of the electron momentum distributions with the increase of the ellipticity and further gain physical insight behind the ellipticity effects in NSDI, it is very helpful to introduce two classifications of the electron trajectories in the context of the semiclassical rescattering scenario. The first classification is based on the travel time of the tunnel-ionized electron before it recollides with the ionic core and gives rise to the occurrence of NSDI [27]. There are two kinds of trajectories: one is single-return collision (SRC) trajectory, which means that the recollision occurs when the tunnel-ionized electron returns to the core for the first time within one optical cycle. The other is multiple-return collision (MRC) trajectory, corresponding to the electrons which recollide with the core after passing the core more than once. The electron from SRC trajectory has less travel time than the one from MRC.

The second classification is based on the laser phase at which electron recollision occurs and one can also define two types of electron trajectories. One is $0.25T$ (here T denotes the optical period) collision trajectory, for which the electron recollision occurs at a time close to $nT + 0.25T$ where n is an integer. Another is the $0.75T$ collision trajectory, corresponding to electron recollision occurring at a laser phase around $nT + 0.75T$. Upon the assumptions that the NSDI occurs immediately upon electron recollision and the initial electron momenta are zero, the electron recollision phase

determines the final state electron momenta directly. For $0.25T$ trajectories, the electrons will acquire a maximal positive momentum from the laser field (note that a cosine waveform laser field is employed in our calculation) and be distributed in the first quadrant. In contrast, the electron pairs from $0.75T$ collision trajectory will contribute to the NSDI events in the third quadrant.

For the linearly polarized laser field ($\varepsilon = 0$), due to the quantum wave packet's transverse spread, the first electron from SRC trajectory should have more chance than that from MRC to collide with the core and to dislodge the second bounded electron. It is thus expected that NSDI probability will decline rapidly with the travel time of the first electron. From a simple kinematic analysis in the context of the simple rescattering scenario, it can be derived that a SRC trajectory with the highest kinetic energy ($E_k = 3.17U_p$, where U_p is the ponderomotive energy of the laser field) upon returning to the core will recollide with the ionic core at an instant close to $0.75T$, producing a pair of electrons distributed in the third quadrant of the correlated momentum spectrum. However, Fig. 2(a) shows that the electron pairs are approximately equally distributed in the first and third quadrants. The reason can be traced to the Coulomb interaction of the tunnel-ionized electron with the parent ion, which is neglected in the simplest version of the rescattering model but is fully considered in our model [19,20]. Part of the transversely spreading electron wave packets can be driven back by the long-range Coulomb force to recollide with the ionic core. This phenomenon, conventionally termed as Coulomb focusing effect [19], has also been found to play a significant role in other strong-field atomic phenomena related to electron rescattering, such as ATI [17,18] and HHG [18]. Due to this Coulomb focusing effect, the MRC trajectory, which leads to the roughly symmetric pattern of electron momentum distribution in Fig. 2(a), contributes significantly to NSDI [19,28]. This Coulomb focusing effect is evidenced in Fig. 3(a), where we show the distributions of the recollision time and the corresponding double electron emission time from

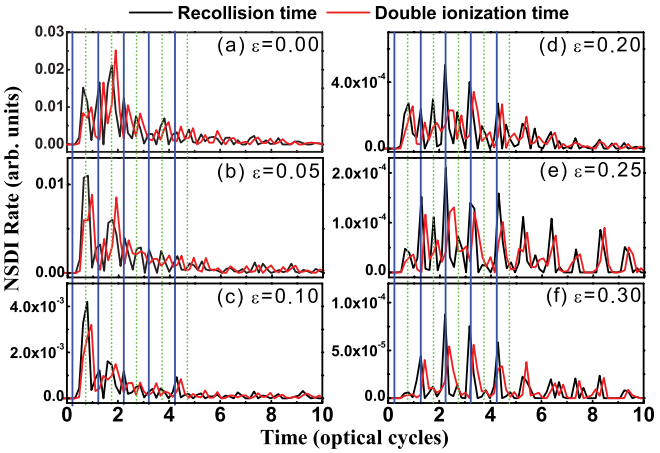

FIG. 3. (Color online) Distributions of recollision time (black lines) and double ionization time (red lines) for different ellipticities. For visual convenience, the first several laser phases corresponding to $0.25T + nT$ and $0.75T + nT$ have been labeled by the vertical blue solid and green dashed lines, respectively. For details, see the text.

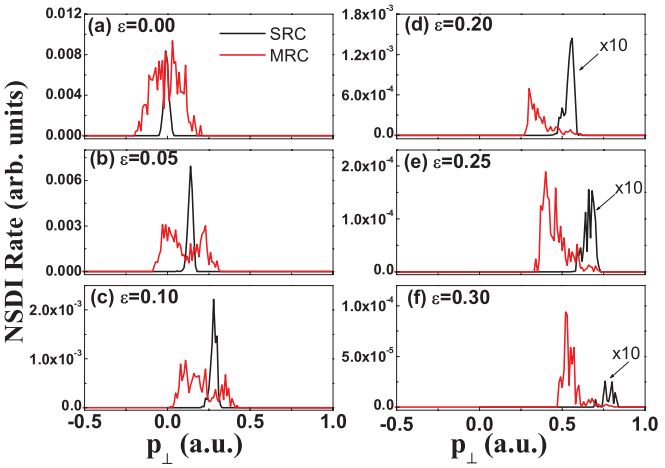

FIG. 4. (Color online) The initial transverse momentum distributions of the first tunnel-ionized electron at various ellipticities, for SRC and MRC trajectories, respectively. Note that for $\varepsilon = 0.20, 0.25$, and 0.30, the contribution from SRC has been multiplied by 10 for visual convenience.

SRC and MRC trajectories, respectively, for linear polarization [29]. Indeed, one finds that the double ionization events from MRC trajectories become comparable to or even more than that from the SRC trajectories, consistent with our analysis above. Also note that, in Fig. 3(a), there always exists a very short time delay (i.e., a small fraction of optical period) between the electron recollision and the NSDI time, irrespective of the SRC or MRC trajectories. This delay is closely related to an attosecond electron thermalization process [30,31] before NSDI occurs.

In order to shed more light on the Coulomb focusing effect in NSDI, we also present in Fig. 4(a) the initial transverse momentum distributions of the tunnel-ionized electrons from SRC and MRC trajectories, respectively, for linear polarization. It is clearly seen that the distribution for SRC trajectories is rather narrow and centers around the origin, while for MRC trajectories the distribution can be much broader. Clearly, the Coulomb focusing effect plays a significant role in driving those trajectories with large initial transverse velocities back to the ionic core.

We now discuss the effect of the ellipticity on NSDI. Compared with the linear polarization, the elliptically polarized laser field has an extra electric field in the transverse direction (e.g., x direction in our case). The extra field component will steer the tunnel-ionized electron away from the ionic core in the transverse direction and results in a dramatic suppression of recollision-induced NSDI. This effect has been demonstrated experimentally by comparing the NSDI yield under various elliptical polarization conditions [6] and has been studied by a semiclassical simulation [12]. However, to our knowledge, the measurement of the differential electron momentum spectrum is not yet achieved [15] and the ellipticity effect on the electron momentum distribution has not been addressed in experiment so far. Our calculation shows that, for relatively small ellipticity, i.e., $\varepsilon = 0.05$ [Fig. 2(b)], the electron pairs are more concentrated in the third quadrant, which is a consequence of the SRC trajectories becoming dominant, and the contribution of the MRC trajectories is largely suppressed,

as shown in Fig. 3(b). When subject to a laser pulse with a small ellipticity, the tunnel-ionized electron must have a proper initial transverse velocity in order to return to the parent ion, as can be seen in Fig. 4(b), which clearly shows a shift of the initial transverse velocity distribution for both SRC and MRC trajectories compared with that of linear polarized laser field. According to Eq. (6), the probability of the trajectory drops with increasing initial transverse velocity, resulting in a decreased probability of both SRC and MRC trajectories in Fig. 4(b) compared with that in Fig. 4(a). On the other side, due to the presence of the additional transverse electric field, the electron wave packet is driven far away from the core in the transverse direction. This effect largely reduces the interaction between the electron and the ionic Coulomb potential. Considering the fact that the contribution of the MRC electrons to NSDI is strongly dependent on the Coulomb focusing effect, the probability of MRC will drop faster with increasing ellipticity than that of the SRC, which is reduced mainly due to the shift of the initial transverse velocity. As a consequence, the SRC electrons become dominant and result in many more electron pairs in the third quadrant than that in the first quadrant, as shown in Fig. 2(b). With further increasing ellipticity (ε increases from 0.05 to 0.10), the initial transverse velocity distributions shift further [see Fig. 4(c)] and the suppression of the Coulomb focusing effect becomes more significant, resulting in a smaller contribution of MRC electrons to NSDI, compared to SRC electrons [comparing Fig. 3(c) with Fig. 3(b)]. In consequence, when $\varepsilon = 0.10$, there are also a majority of electron pairs being concentrated in the third quadrant. Note, however, that the accurate ratio of the total events in the third quadrant with respect to that in the first quadrant is diminished. The reason is that the proportion of MRC belonging to $0.25T$ collision trajectory, which contributes to the NSDI events in the first quadrant, increases for $\varepsilon = 0.10$ compared to $\varepsilon = 0.05$. This tendency becomes more significant with the increasing ellipticity and will be discussed further later.

With further increased ellipticity, however, the contribution from SRC trajectory becomes significantly suppressed, and the ones from MRC reassert their dominance, as shown in Figs. 3(d)–3(f), corresponding to the ellipticities of 0.20, 0.25, and 0.30, respectively. This is because that for the large ellipticities, the transverse component of the laser field gives rise to considerably large amplitude of the electron lateral shift. In order to come back to the parent ion, the initial transverse velocity of tunnel-ionized electron has to be comparatively large to compensate this lateral shift. Moreover, as shown in Ref. [16], the corresponding initial transverse velocity of the SRC electron needs to be significantly lager than that of the MRC electron. This can also be clearly seen in Figs. 4(d)–4(f), which show that, with the increase in ellipticity, the initial transverse velocity of the SRC electron is larger and larger than and separated from that of the MRC electron. Note that the Coulomb focusing effect for MRC is also further suppressed with the increase of the laser ellipticity, which is reflected in Figs. 4(d)–4(f) by the fact that the width of initial transverse velocity distribution for MRC decreases with the increasing ellipticity. However, since the probability of the trajectory is exponentially decreasing with the increase of initial transverse velocity [see Eq. (6)], the suppression of the

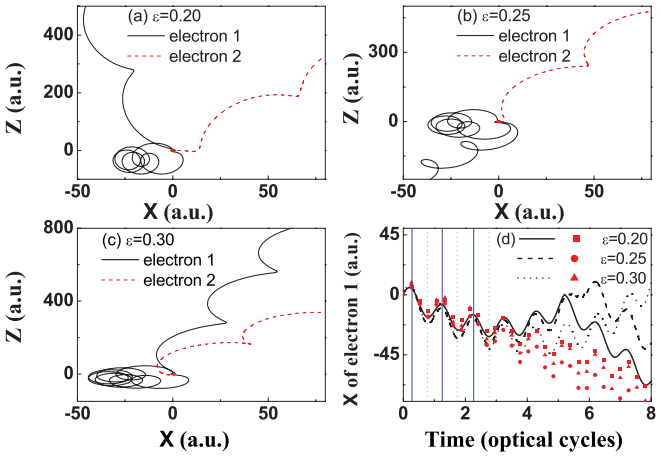

FIG. 5. (Color online) (a)–(c) Typical recollision trajectories for $\varepsilon = 0.20$, $\varepsilon = 0.25$, and $\varepsilon = 0.30$. The black (solid) and red (dashed) curves represent the trajectories of electrons 1 and 2, respectively. (d) The evolution of the transverse distance of the tunnel-ionized electrons as a function of the time for the three recollision trajectories in (a)–(c). The black solid, dashed, and dotted curves show the evolution for $\varepsilon = 0.20$, 0.25, and 0.30, respectively, when the Coulomb potential is included, while for the red curves with symbols (solid squares, solid circles, and solid triangles), the Coulomb potential is not considered. The vertical solid and dashed lines have the same meanings as in Fig. 3.

SRC contribution due to its large initial transverse velocity can overwhelm the suppression of MRC related to the Coulomb focusing effect. As a consequence, the contribution of the MRC electron becomes dominating and the SRC contribution electron is more and more suppressed, relatively. This is in agreement with the analysis of Ref. [16] that the contribution from MRC trajectory becomes more significant than that from SRC trajectory when the ellipticity is large.

A closer inspection of Figs. 3(d)–3(f) reveals another pronounced feature: With the increase of the ellipticity, the $0.25T$ collision trajectory surpasses remarkably the $0.75T$ collision trajectory for MRC electrons. This, together with the fact that SRC gradually loses its significance to NSDI events, accounts well for the observation in Figs. 2(d)–2(f): More and more electron pairs are accumulated in the first quadrant when the ellipticity increases from 0.20 to 0.30. In order to understand this critical change of the collision time of MRC trajectories with ellipticity, we plot in Figs. 5(a)–5(c) typical NSDI electron trajectories in the polarization plane for $\varepsilon = 0.20$, 0.25, and 0.30, respectively. It can be seen that, different from trajectories depicted in Fig. 2 of Ref. [16], which circle around the core for one or more cycles and finally return to the core, the tunnel-ionized electron initially moves to the right half space ($x > 0$), being driven back to the left half space ($x < 0$), and circles in the left half space for several cycles. The electron then gradually moves in the positive direction and returns to collide with the core to ionize the second bound electron eventually. This different behavior of the electron trajectory is obviously related to the ionic Coulomb potential, which is completely neglected in Ref. [16] but has been taken into account in a completely classical treatment [11]. To clearly illustrate the significant role of the ionic Coulomb potential,

we further plot in Fig. 5(d) the evolution of the tunnel-ionized electron in the transverse direction as a function of time, with and without the Coulomb potential included. When the Coulomb potential is considered (see the black solid, dashed and dotted curves in Fig. 5(d) for $\varepsilon = 0.20$, 0.25, and 0.30, respectively), one sees that at the very beginning, all three of these trajectories are driven away from the origin by the transverse field. However, after several optical cycles, the electron is gradually pulled back by the ionic Coulomb potential. In contrast, when the Coulomb potential is omitted [see the red curves with symbols in Fig. 5(d)], the tunnel-ionized electrons will be driven away from and never come back to the ionic core. It is noteworthy that in each optical cycle, the electron's lateral shift reaches a minimum at about the times of $nT + 0.25T$ but reaches a maximum at about the times of $nT + 0.75T$. Therefore, the $0.25T$ collision trajectory is enhanced and the $0.75T$ collision trajectory is significantly suppressed with the increasing ellipticity. As a consequence, the electron pairs will be more and more distributed in the first quadrant.

Note that, from an experimental point of view, the results shown in Fig. 2, i.e., the distinct evolution of the correlated electron momentum distributions with ellipticity, may not be accessible in experiments since only the electron tunneling out in the first half cycle of the pulse is considered in the calculation. The asymmetric distribution shown in Fig. 2 will become symmetrical when electrons tunneled from the other half cycle of the laser pulse are included in the calculation. In order to relate our theoretical predictions more closely to the reality, we further perform a calculation which considers *both* half cycles but restricts both electrons' transverse momenta, i.e., p_x, to positive values, adopting the same procedure as in Ref. [16]. Experimentally, the longitudinal electron momentum distribution with restricted range of transverse momentum has been routinely employed in the analysis of the data in the COLTRIMS experiments [32,33].

The calculated correlated electron momentum distributions are depicted in Figs. 6(a)–6(f). Some intriguing features are noticeable. For $\varepsilon = 0$, the proportions of electron pairs in the first and third quadrants are nearly the same as expected [16]. When the ellipticity increases to $\varepsilon = 0.25$, more and more electron pairs appear in the first quadrant than in the third quadrant. However, from $\varepsilon = 0.25$ to $\varepsilon = 0.30$, although more electron pairs still accumulate in the first quadrant, the ratio of W_{1st} to W_{3rd} decreases. Nevertheless, the asymmetry in the momentum distribution is preserved for a full optical cycle, which should be accessible to a realistic experiment.

In order to show the nontrivial evolution in Figs. 6(a)–6(f) with the increase of the ellipticity more clearly, the asymmetry parameter α applied in Ref. [16] can be used here. α is defined as

$$\alpha = \frac{W_{1st} - W_{3rd}}{W_{1st} + W_{3rd}}. \tag{7}$$

In Fig. 6(g) we plot the asymmetry parameter α as a function of ellipticity. It shows that when $\varepsilon \leqslant 0.25$, α increases from about 0 to 0.68, indicating that the electron pairs accumulate in the first quadrant. However, when ε increases to 0.30, α decreases to 0.5, which means that the electron pairs start to move to the third quadrant again. This tendency is consistent with Fig. 8 in Ref. [16]. Note that the maximum of α in our result is much larger (more than three times) than that in Ref. [16], which is apparently due to the Coulomb potential which is ignored in the SFA calculation but plays an important role in the NSDI dynamics in an elliptically polarized laser field. More importantly, this asymmetry feature as a function of ellipticity could be directly tested by an experiment with the help of COLTRIMS apparatus in the near future.

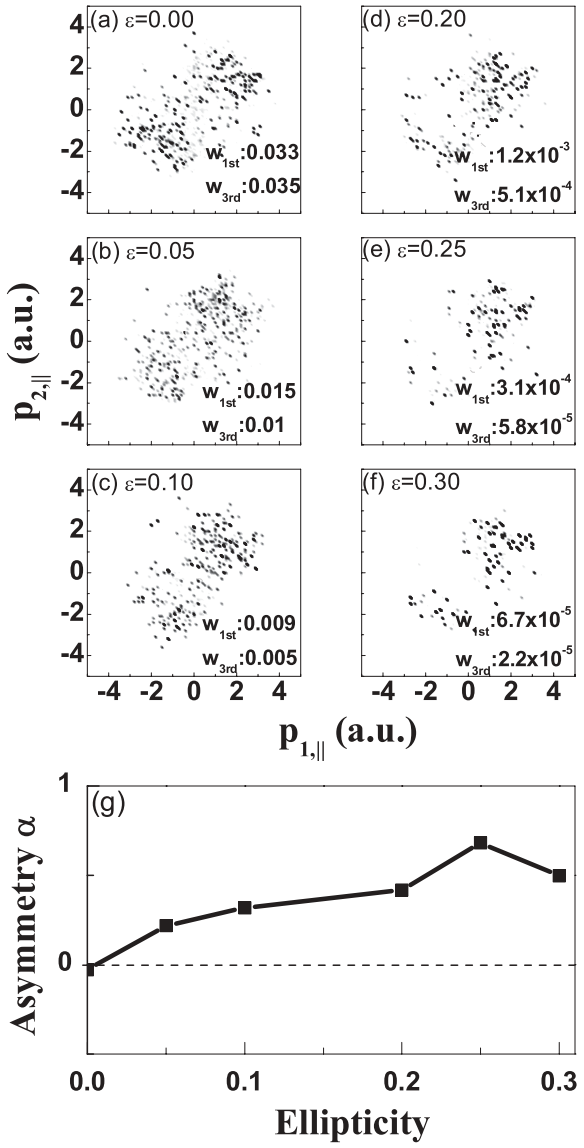

FIG. 6. (a)–(f) Correlated electron momentum distributions by restricting both electrons' p_x to positive values for various ellipticities. W_{1st} and W_{3rd} represent the total weights of electron pairs in the first and third quadrants, respectively. (g) Asymmetry parameter α as a function of ellipticity.

IV. CONCLUSIONS

In conclusion, we have investigated NSDI dynamics of the noble gas neon subject to intense elliptically polarized laser fields with a semiclassical model. Depending on the laser ellipticity, either SRC or MRC trajectory will dominate, resulting in a distinct shift of the correlated momentum distribution between the first and the third quadrants in the

correlated momentum plane. This change can be understood by the interplay between the effects of the transverse electric field and the ionic Coulomb potential on the evolution of the first tunnel-ionized electron. With small ellipticity, the tunnel-ionized electron will drift far away from the ionic core in the transverse direction by the additional minor field. In order to return back to the ionic core, the initial transverse velocity of the electron has to shift to compensate the lateral shift. This leads to a decreased double-ionization probability for both SRC and MRC trajectories. Furthermore, the Coulomb focusing effect, which plays a significant role in MRC trajectory, is suppressed to some extent, resulting in the main contribution of the SRC trajectory in NSDI events and the concentration of the electron pairs in the third quadrant in the correlated electron momentum plane. In contrast, with large ellipticities, the SRC trajectory has to possess a very large initial transverse velocity in order to return and collide with the ionic core and its contribution is becoming dramatically suppressed. For MRC trajectory, the initial transverse velocity for compensation is relatively small and the Coulomb potential can still pull back the electron to collide with the core. As a consequence, MRC trajectory may reassert its dominance in producing NSDI events. Especially, most of the MRC trajectory will recollide with the ionic core at a time corresponding to $nT + 0.25T$, resulting in the correlated electron momentum distribution mainly in the first quadrant. Moreover, to relate our theoretical prediction more closely to experimental reality, we calculate the correlated electron momentum distributions for one full optical cycle and restrict the final drift momentum of both electrons p_x to positive values. In this case, the asymmetry parameter describing the asymmetry of momentum distributions in the first and third quadrants increases with ellipticity and then decreases at large ellipticities ($\varepsilon > 0.25$ in our case). This abnormal feature may be tested in a COLTRIMS experimental measurement in the near future. In addition, the maximal asymmetry parameter from our model calculation is considerably larger than that predicted by the SFA calculation, reflecting the important role of the Coulomb potential in the NSDI dynamics.

ACKNOWLEDGMENTS

This work is supported by NNSF of China (Grants No. 10925420, No. 11074026, No. 11174330, and No. 11274050) and the National Basic Research Program of China Grants (No. 2011CB8081002 and No. 2013CB922200).

[1] M. Protopapas, C. H. Keitel, and P. L. Knight, Rep. Prog. Phys. **60**, 389 (1997).
[2] W. Becker and H. Rottke, Contemp. Phys. **49**, 199 (2008).
[3] C. Figueira de Morisson Faria and X. Liu, J. Mod. Opt. **58**, 1076 (2011).
[4] W. Becker, X. Liu, P. Ho, and J. H. Eberly, Rev. Mod. Phys. **84**, 1011 (2012).
[5] P. B. Corkum, Phys. Rev. Lett. **71**, 1994 (1993).
[6] P. Dietrich, N. H. Burnett, M. Ivanov, and P. B. Corkum, Phys. Rev. A **50**, R3585 (1994).
[7] C. Guo, M. Li, J. P. Nibarger, and G. N. Gibson, Phys. Rev. A **58**, R4271 (1998).
[8] C. Guo and G. N. Gibson, Phys. Rev. A **63**, 040701 (2001).
[9] G. D. Gillen, M. A. Walker, and L. D. Van Woerkom, Phys. Rev. A **64**, 043413 (2001).
[10] X. Wang and J. H. Eberly, Phys. Rev. Lett. **105**, 083001 (2010).
[11] X. Wang and J. H. Eberly, New J. Phys. **12**, 093047 (2010).
[12] X. L. Hao, G. Q. Wang, X. Y. Jia, W. D. Li, J. Liu, and J. Chen, Phys. Rev. A **80**, 023408 (2009).
[13] L. B. Fu, G. G. Xin, D. F. Ye, and J. Liu, Phys. Rev. Lett. **108**, 103601 (2012).
[14] J. Ullrich, R. Moshammer, A. Dorn, R. Dörner, L. Ph. Schmidt, and H. Schmidt-Böcking, Rep. Prog. Phys. **66**, 1463 (2003).
[15] Note that a differential momentum distribution of the doubly charged recoil ion from double ionization of Ar and Ne in an intense circularly polarized laser field has been recorded by C. M. Maharjan, A. S. Alnaser, X. M. Tong, B. Ulrich, P. Ranitovic, S. Ghimire, Z. Chang, I. V. Litvinyuk, and C. L. Cocke, Phys. Rev. A **72**, 041403(R) (2005). However, the experiment was performed in the sequential ionization regime.
[16] N. I. Shvetsov-Shilovski, S. P. Goreslavski, S. V. Popruzhenko, and W. Becker, Phys. Rev. A **77**, 063405 (2008).
[17] W. Quan, Z. Lin, M. Wu, H. Kang, H. Liu, X. Liu, J. Chen, J. Liu, X. T. He, S. G. Chen, H. Xiong, L. Guo, H. Xu, Y. Fu, Y. Cheng, and Z. Z. Xu, Phys. Rev. Lett. **103**, 093001 (2009).
[18] W. Chu, M. Wu, B. Zeng, J. Yao, J. Ni, H. Xiong, H. Xu, Z. Lin, H. Kang, W. Quan, J. Chen, X. Liu, Y. Cheng, and Z. Xu, Phys. Rev. A **85**, 021403(R) (2012).
[19] T. Brabec, M. Y. Ivanov, and P. B. Corkum, Phys. Rev. A **54**, R2551 (1996).
[20] J. Chen, J. Liu, L. B. Fu, and W. M. Zheng, Phys. Rev. A **63**, 011404(R) (2000); L. B. Fu, J. Liu, J. Chen, and S. G. Chen, *ibid.* **63**, 043416 (2001); J. Chen, J. Liu, and W. M. Zheng, *ibid.* **66**, 043410 (2002); D. F. Ye, X. Liu, and J. Liu, Phys. Rev. Lett. **101**, 233003 (2008).
[21] N. B. Delone and V. P. Krainov, J. Opt. Soc. Am. B. **8**, 1207 (1991).
[22] L. D. Landau *et al.*, *Quantum Mechanics* (Pergamon, New York, 1977).
[23] J. S. Cohen, Phys. Rev. A **26**, 3008 (1982).
[24] C. F. Faria, X. Liu, A. Sanpera, and M. Lewenstein, Phys. Rev. A **70**, 043406 (2004).
[25] C. Figueira de Morisson Faria, H. Schomerus, X. Liu, and W. Becker, Phys. Rev. A **69**, 043405 (2004).
[26] X. Liu and C. Figueira de Morisson Faria, Phys. Rev. Lett. **92**, 133006 (2004).
[27] X. L. Hao, W. D. Li, J. Liu, and J. Chen, Phys. Rev. A **83**, 053422 (2011).
[28] V. R. Bhardwaj, S. A. Aseyev, M. Mehendale, G. L. Yudin, D. M. Villeneuve, D. M. Rayner, M. Yu. Ivanov, and P. B. Corkum, Phys. Rev. Lett. **86**, 3522 (2001).

[29] The recollision time is defined as the moment that the two electrons after tunneling have the closest distance, while the double ionization time is determined by the instant at which both electrons possess positive energy.

[30] X. Liu, C. Figueira de Morisson Faria, W. Becker, and P. B. Corkum, J. Phys. B **39**, L305 (2006).

[31] X. Liu, C. Figueira de, Morisson Faria, and W. Becker, New J. Phys. **10**, 025010 (2008).

[32] M. Weckenbrock, M. Hattass, A. Czasch, O. Jagutzki, L. Schmidt, T. Weber, H. Roskos, T. Löffler, M. Thomson, and R. Dörner, J. Phys. B **34**, L449 (2001).

[33] R. Moshammer, B. Feuerstein, J. Crespo López-Urrutia, J. Deipenwisch, A. Dorn, D. Fischer, C. Höhr, P. Neumayer, C. D. Schröter, J. Ullrich, H. Rottke, C. Trump, M. Wittmann, G. Korn, and W. Sandner, Phys. Rev. A **65**, 035401 (2002).